PERGAMON

International Journal of Heat and Mass Transfer 43 (2000) 2641–2655

International Journal of HEAT and MASS TRANSFER

www.elsevier.com/locate/ijhmt

Transient characterization of flat plate heat pipes during startup and shutdown operations

Y. Wang, K. Vafai*

Department of Mechanical Engineering, The Ohio State University, Columbus, OH 43210-1107, USA

Received 23 September 1999; received in revised form 20 January 2000

Abstract

Analytical models for predicting the transient performance of a flat plate heat pipe for startup and shutdown operations are developed in this work. These models can be utilized separately for a startup or a shutdown operation, respectively. The two models can also be combined together to simulate the thermal performance of a flat plate heat pipe in cyclical startup and shutdown operations. The transient temperature distributions in the heat pipe walls and wicks are presented in this work. The results reveal that the thermal diffusivity, the thickness of the wall and the wick, and the heat input pattern affect the heat pipe time constants. The wicks create the main thermal resistance resulting in the largest temperature drop in the heat pipe, thus substantially influencing the performance of the heat pipe.

Keywords: Flat-shaped heat pipes; Startup and shutdown; Transient characteristics

1. Introduction

Flat plate heat pipes have attracted substantial attention lately due to their advantages over conventional cylindrical heat pipes, such as geometry adaptation, ability for very localized heat dissipation, and the production of an entirely flat isothermal surface. Due to these advantages, flat plate heat pipes have become increasingly attractive for various applications such as the cooling of electronic devices [1] and space vehicles [2].

A few analytical models and simulations for conventional cylindrical heat pipe mainly concentrate on the startup operation involving liquid metal working fluids [3,4]. In these analytical works, a lumped one-dimensional model is utilized. Furthermore, in order to simplify the complicated problem, the temperature difference across the heat pipe walls and wicks are neglected in these transient models [3,4]. Detailed analytical models and simulations for a flat plate heat pipe were presented by Vafai et al. [5,6]. The liquid flow in the porous wicks and the vapor flow in the vapor region were first established by Vafai and Wang [5] and were later modified by Vafai et al. [6]. In these works, both analytical and numerical methods were utilized. Zhu and Vafai [7] utilized both analytical and numerical methods to study the three-dimensional vapor flow in the vapor channel as well as the analysis of the liquid flow through the porous wicks. The results reveal that vapor velocity profiles are non-similar and asymmetrical. Vapor flow reversal was observed along the top condenser region. It is found that the transverse pressure variations are relatively small and can be neglected.

To predict the transient heat transfer across the heat

* Corresponding author. Tel.: +1-614-292-6560; fax: +1-614-292-3163.

E-mail address: vafai.1@osu.edu (K. Vafai).

0017-9310/00/$ - see front matter
PII: S0017-9310(99)00295-1

Nomenclature

A	heat input area, m^2
c	specific heat, J/(kg °C)
h	thickness, m
h_{conv}	heat transfer coefficient, W/(m^2 °C)
H	height of the heat pipe, m
k	thermal conductivity, W/(m °C)
L	half length of the heat pipe, m
L_e	half width of heater
q	heat flux, W/m^2
Q	power input rate, W
t	time, s
t_c	time constant, s
T	temperature, °C
W	width of the heat pipe, m
y	normal coordinate
z	normal coordinate
δ	temperature penetration depth, m
ρ	density, kg/m^3
ΔT	temperature difference, °C
ε	porosity
θ	temperature rise, °C

Subscripts

1	wall of evaporator section
2	wick of evaporator section
3	wick of condenser section
4	wall of condenser section
c	condenser
e	evaporator
eff	effective
l	liquid
max	maximum
oc	outside surface of the condenser section
oe	outside surface of the evaporator section
s	solid
v	vapor
w	wick
wa	wall
wv	wick–vapor interface
ww	wall–wick interface
∞	environment

pipe walls and wicks and the temperature distributions in the heat pipe, Zhu and Vafai [8] developed a mathematical model for a flat plate heat pipe for a startup operation. In their work, the thermal performance of a flat plate heat pipe in the shutdown operation was not addressed. To the best of our knowledge, there is no other analytical work addressing the heat transfer and temperature distributions within a flat plate heat pipe open in the literature. Also, there is no analytical work on the transient performance of a flat plate heat pipe during the shutdown operation reported in the literature.

In the present study, a physical model for the flat plate heat pipe is introduced. Based on the physical model, analytical results for the temperature distribution and heat transfer are developed and simulated for predicting the transient performance of a flat plate heat pipe for both the startup and shutdown operations. The results are discussed in detail in this work.

2. Physical model

The schematic of a flat plate heat pipe is shown in Fig. 1. During the operation of a flat plate heat pipe, heat is transferred through the heat pipe walls by conduction. In the porous wick of the evaporator section, there is heat conduction in the metal matrix, liquid flow through the pores, and evaporation at the wick–vapor interface. Within the wick of the condenser section, there is conduction in the metal matrix, liquid flow inside the pores and condensation at the vapor–wick interface. The details of the fluid flow in the wicks and the vapor dynamics have been considered in detail by Vafai et al. [5–7] and will not be addressed here.

A heat conduction model for the wicks is utilized in this work. The main assumptions are:

1. The heat transfer in the wick is by conduction with an effective thermal conductivity, $k_w = k_{eff}$, effective diffusivity, $\alpha_w = \alpha_{eff}$, effective density, ρ_{eff}, and effective specific heat, c_{eff}.
2. The temperature in the vapor phase is uniform at any time.
3. The thermal properties of the heat pipe wall and the wick are taken to be constant.

3. Model description for the startup operation

The coordinates utilized in this work are shown in Fig. 2. Various temperatures are measured relative to the initial temperature. These are given as

$$\theta_{wa,\,e}(t, y_1) = T_{wa,\,e}(t, y_1) - T_i \tag{1}$$

$$\theta_{w,\,e}(t, y_2) = T_{w,\,e}(t, y_2) - T_i \tag{2}$$

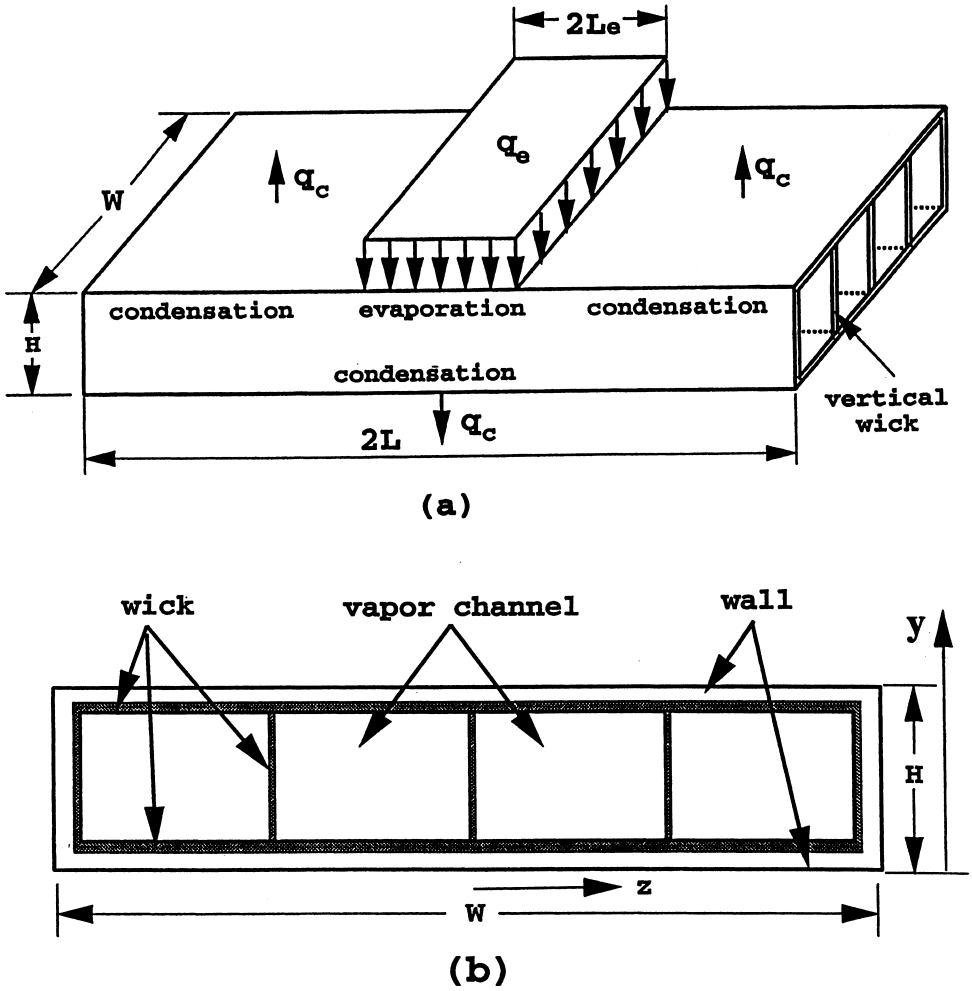

Fig. 1. Schematic of the flat plate heat pipe: (a) geometry of the heat pipe, (b) cross sectional view of the heat pipe.

$$\theta_{w,\,c}(t, y_3) = T_{w,\,c}(t, y_3) - T_i \tag{3}$$

$$\theta_{wa,\,c}(t, y_4) = T_{wa,\,c}(t, y_4) - T_i \tag{4}$$

3.1. Initial conditions

At $t = 0$, the temperature is uniform everywhere over the entire heat pipe and equals to its initial temperature, T_i. Therefore, the temperature rise in the heat pipe walls and the wicks is

$$\theta_{wa,\,e}(t, y_1) = 0 \tag{5}$$

$$\theta_{w,\,e}(t, y_2) = 0 \tag{6}$$

$$\theta_{w,\,c}(t, y_3) = 0 \tag{7}$$

$$\theta_{wa,\,c}(t, y_4) = 0 \tag{8}$$

3.2. Temperature variations within the evaporator section

3.2.1. $0 < \delta_1 < h_{wa}$

After the initial application of the input power, the temperature front will first progress through the evaporator wall. During this step, the temperature front marches from the outside wall surface to the wall–wick interface of the evaporator section. In this phase, there is no temperature rise in the wicks or in the wall in the condenser section. The temperature distribution in the heat pipe wall in the evaporator section is taken as

$$\theta_{wa,\,e}(t, y_1) = a_1(t) + b_1(t)y_1 + c_1(t)y_1^2 \tag{9}$$

The corresponding boundary conditions are

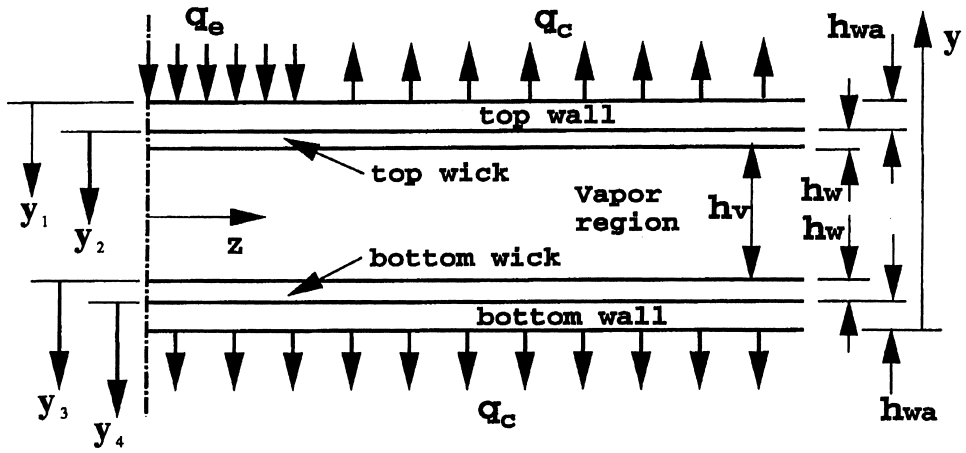

Fig. 2. Coordinate systems used in the analysis.

$$y_1 = 0, \quad q_e = -k_{wa}\frac{\partial \theta_{wa,\,e}(t, y_1)}{\partial y_1} \tag{10}$$

$$y_1 = \delta_1(t), \quad \theta_{wa,\,e}(t, y_1) = 0 \tag{11}$$

$$y_1 = \delta_1(t), \quad \frac{\partial \theta_{wa,\,e}(t, y_1)}{\partial y_1} = 0 \tag{12}$$

Satisfying the boundary condition (10)–(12) in Eq. (9) results

$$a_1(t) = \frac{q_e \delta_1(t)}{2k_{wa}}, \quad b_1(t) = -\frac{q_e}{k_{wa}}, \quad c_1(t) = \frac{q_e}{2k_{wa}\delta_1(t)} \tag{13}$$

Therefore, the temperature distribution in the wall of the evaporator section is

$$\theta_{wa,\,e}(t, y_1) = \frac{q_e \delta_1(t)}{2k_{wa}}\left(1 - \frac{y_1}{\delta_1(t)}\right)^2 \tag{14}$$

The only unknown in Eq. (14) is $\delta_1(t)$, which can be determined by integrating the heat conduction equation, i.e.,

$$\int_0^{\delta_1(t)} \frac{\partial \theta_{wa,\,e}(t, y_1)}{\partial t}\,dy_1 = \int_0^{\delta_1(t)} \alpha_{wa}\frac{\partial^2 \theta_{wa,\,e}(t, y_1)}{\partial^2 y_1}\,dy_1 \tag{15}$$

Substituting Eq. (14) into (15) yields

$$d\delta_1^2(t) = 6\alpha_{wa}\,dt \tag{16}$$

Integrating Eq. (16) yields the thermal front layer thickness

$$\delta_1 = \sqrt{6\alpha_{wa}t} \tag{17}$$

3.2.2. $0 \le \delta_2(t) \le h_w$

The temperature front moves further inside the heat pipe during this time period. At the end of this period, the temperature front reaches the wick–vapor interface of the evaporator section. During this step, the temperature does not change in the condenser section. The temperature rises in the heat pipe wall and in the wick of the evaporator section are taken as

$$\theta_{wa,\,e}(t, y_1) = a_1(t) + b_1(t)y_1 + c_1(t)y_1^2 \tag{18}$$

$$\theta_{w,\,e}(t, y_2) = a_2(t) + b_2(t)y_2 + c_2(t)y_2^2 \tag{19}$$

The boundary conditions for the heat pipe wall of the evaporator section, for this period, are

$$y_1 = 0, \quad q_e = -k_{wa}\frac{\partial \theta_{wa,\,e}(t, y_1)}{\partial y_1} \tag{20}$$

$$y_1 = h_{wa}, \quad \theta_{wa,\,e}(t, y_1) = \theta_{ww,\,e}(t) \tag{21}$$

$$y_1 = h_{wa}, \quad q_{ww,\,e}(t) = -k_{wa}\frac{\partial \theta_{wa,\,e}(t, y_1)}{\partial y_1} \tag{22}$$

where, $\theta_{ww,\,e}(t)$ and $q_{ww,\,e}(t)$ are temperature rise and heat flux in the wall–wick interface of the evaporator section, respectively. According to the physical model discussed previously, the boundary conditions for the wick of the evaporator section are

$$y_2 = 0, \quad \theta_{w,\,e}(t, y_2) = \theta_{ww,\,e}(t) \tag{23}$$

$$y_2 = \delta_2(t), \quad \theta_{w,\,e}(t, y_2) = 0 \tag{24}$$

$$y_2 = \delta_2(t), \quad \frac{\partial \theta_{w,e}(t, y_2)}{\partial y_2} = 0 \tag{25}$$

Applying boundary conditions, Eqs. (20)–(22), to Eq. (18) yields the temperature distribution in the heat pipe wall in the evaporator section:

$$\theta_{wa,e}(t, y_1) = \theta_{ww,e}(t) + \frac{[q_e + q_{ww,e}(t)]h_{wa}}{2k_{wa}} - \frac{q_e}{k_e}y_1 + \left[\frac{q_e - q_{ww,e}(t)}{2k_{wa}h_{wa}}\right]y_1^2 \tag{26}$$

Applying boundary conditions, Eqs. (23)–(25), to Eq. (19) yields the temperature distribution in the wick of the evaporator section:

$$\theta_{w,e}(t, y_2) = \theta_{ww,e}(t)\left[1 - \frac{y_2}{\delta_2(t)}\right]^2 \tag{27}$$

There are three unknowns in Eqs. (26) and (27), i.e., θ_{ww}, $e(t)$, q_{ww}, $e(t)$, and $\delta_2(t)$. These 3 unknowns should be determined by utilizing overall energy balances and the continuity of heat flux in the heat pipe wall–wick interface in the evaporator section. In the heat pipe wall–wick interface in the evaporator section,

$$y_2 = 0, \quad q_{ww,e}(t) = -k_w \frac{\partial \theta_{w,e}(t, y_2)}{\partial y_2} \tag{28}$$

Substituting Eq. (27) into (28) yields

$$q_{ww,e}(t) = \frac{2k_{ww,e}\theta_{ww,e}(t)}{\delta_2(t)} \tag{29}$$

The overall energy balance equation for the wick of the evaporator section is

$$\int_0^{\delta_2(t)} \frac{\partial \theta_{w,e}(t, y_2)}{\partial t}\,dy_2 = \int_0^{\delta_2(t)} \alpha_w \frac{\partial^2 \theta_{w,e}(t, y_2)}{\partial y_2^2}\,dy_2 \tag{30}$$

Introducing Eq. (27) into (30) yields

$$\frac{d}{dt}\left[\delta_2(t)\theta_{ww,e}(t)\right] = \frac{6\alpha_w \theta_{ww,e}(t)}{\delta_2(t)} \tag{31}$$

The overall energy balance equation in the heat pipe wall of the evaporator section is

$$\int_0^{h_{wa}} \frac{\partial \theta_{wa,e}(t, y_1)}{\partial t}\,dy_1 = \int_0^{h_{wa}} \alpha_{wa} \frac{\partial^2 \theta_{wa,e}(t, y_1)}{\partial y_1^2}\,dy_1 \tag{32}$$

Substituting Eq. (26) into (32) results in

$$\frac{d\theta_{ww,e}(t)}{dt} + \frac{h_{wa}}{3k_{wa}}\frac{dq_{ww,e}(t)}{dt} = \frac{\alpha_{wa}\lfloor q_e - q_{ww,e}(t)\rfloor}{k_{wa}h_{wa}} \tag{33}$$

Therefore, the three unknowns in Eqs. (26) and (27), θ_{ww}, $e(t)$, q_{ww}, $e(t)$, and $\delta_2(t)$, can be determined uniquely by solving Eqs. (29), (31) and (33).

3.3. Temperature variations within the condenser section

3.3.1. $0 \le \delta_3(t) \le h_w$

During this time period, there is no temperature change in the heat pipe wall in the condenser section and the temperature rise in the heat pipe wall in the evaporator section is given by Eq. (26). The temperature distribution in the wick in the evaporator section and that in the wick in the condenser section are taken as

$$\theta_{w,e}(t, y_2) = a_2(t) + b_2(t)y_2 + c_2(t)y_2^2 \tag{34}$$

and

$$\theta_{w,c}(t, y_3) = a_3(t) + b_3(t)y_3 + c_3(t)y_3^2 \tag{35}$$

The boundary conditions for the wick in the evaporator section are

$$y_2 = 0, \theta_{w,e}(t, y_2) = \theta_{ww,e}(t) \tag{36}$$

$$y_2 = 0, \quad q_{ww,e}(t) = -k_w \frac{\partial \theta_{w,e}(t, y_2)}{\partial y_2} \tag{37}$$

$$y_2 = h_w, \quad \theta_{w,e}(t, y_2) = \theta_v(t) \tag{38}$$

and the boundary conditions for the bottom wick in the condenser section are

$$y_3 = 0, \quad \theta_{w,c}(t, y_3) = \theta_v(t) \tag{39}$$

$$y_3 = \delta_3(t), \quad \theta_{w,c}(t, y_3) = 0 \tag{40}$$

$$y_3 = \delta_3(t), \quad \frac{\partial \theta_{w,c}(t, y_3)}{\partial y_3} = 0 \tag{41}$$

where, $\theta_v(t)$ is the vapor temperature rise, $\theta_{ww,e}(t)$, and $q_{ww,e}(t)$ are the temperature rise and the heat flux in the wall–wick interface of the evaporator section, respectively. Applying boundary conditions, Eqs. (36)–(38), to Eq. (34) yields the temperature distribution in the wick in the evaporator section

$$\theta_{w,e}(t, y_2) = \theta_{ww,e}(t) - \frac{q_{ww,e}(t)}{k_w}y_2 + \left[\frac{q_{ww,e}(t)}{k_{wa}h_{wa}} - \frac{\theta_{ww,e}(t) - \theta_v(t)}{h_w^2}\right]y_2^2 \tag{42}$$

Applying boundary conditions, Eqs. (39)–(41), to Eq. (35) yields the temperature distribution in the wick in

the condenser section:

$$\theta_{w,\,c}(t, y_3) = \theta_v(t)\left[1 - \frac{y_3}{\delta_3(t)}\right]^2 \tag{43}$$

The temperature distributions for the wall and wick of the evaporator section and the wick of the condenser section are given by Eqs. (26), (42) and (43). There are four unknowns, i.e., θ_{ww}, $e(t)$, q_{ww}, $e(t)$, $\theta_v(t)$, and $\delta_3(t)$, in these equations. These four unknowns can be determined by global energy balances and application of the continuity of heat flux and the temperature at the interfaces. The energy balance equation for the wick in the evaporator section is

$$\int_0^{h_w} \frac{\partial \theta_{w,\,e}(t, y_2)}{\partial t}\,dy_2 = \int_0^{h_w} \alpha_w \frac{\partial^2 \theta_{w,\,e}(t, y_2)}{\partial y_2^2}\,dy_2 \tag{44}$$

Substituting Eq. (42) into Eq. (44) yields

$$\frac{2}{3}\frac{d\theta_{ww,\,e}(t)}{dt} + \frac{1}{3}\frac{d\theta_v(t)}{dt} - \frac{h_w}{6k_w}\frac{dq_{ww,\,e}(t)}{dt} = \frac{2\alpha_w}{k_w h_w}\left[q_{ww,\,e}(t) - \frac{k_w\left(\theta_{ww,\,e}(t) - \theta_v(t)\right)}{h_w}\right] \tag{45}$$

The energy leaving the wick of the evaporator section equals that entering the wick of the condenser section. Thus, we have the following relation:

$$q_{wv,\,e}(t) = \frac{q_{wv,\,c}(t) A_c}{A_e} \tag{46}$$

where, A_e is the evaporator area and A_c is the entire condenser area, including the top and bottom sections. It should be noted that $q_{wv,\,e}$ and $q_{wv,\,c}$ are not used directly in the above set of equations, rather they are translated through the use of Eqs. (42) and (43). The energy balance for the bottom wick in the condenser section is

$$\int_0^{\delta_3(t)} \frac{\partial \theta_{w,\,c}(t, y_3)}{\partial t}\,dy_3 = \int_0^{\delta_3(t)} \alpha_w \frac{\partial^2 \theta_{w,\,c}(t, y_3)}{\partial y_3^2}\,dy_3 \tag{47}$$

Substituting Eq. (43) into (47) and rearranging yields

$$\frac{d}{dt}\left[\delta_3(t)\theta_v(t)\right] = \frac{6\alpha_w \theta_v(t)}{\delta_3(t)} \tag{48}$$

The energy balance for the heat pipe wall in the evaporator section is Eq. (33). Therefore, the four unknowns, θ_{ww}, $e(t)$, q_{ww}, $e(t)$, $\theta_v(t)$, and $\delta_3(t)$ can be determined by solving Eqs. (33), (45), (46) and (48) simultaneously. The temperature distributions of the evaporator section and the wick of the condenser section, i.e., Eqs. (26), (42), and (43), can then be determined uniquely.

3.3.2. $0 \le \delta_4(t) \le h_{wa}$

During this period, the temperature distributions in the evaporator section for the heat pipe wall and the wick are prescribed by Eqs. (26) and (42), respectively. The temperature distribution within the wick of condenser section is taken as

$$\theta_{w,\,c}(t, y_3) = a_3(t) + b_3(t) y_3 + c_3(t) y_3^2 \tag{49}$$

and for the wall of the condenser section is taken as

$$\theta_{wa,\,c}(t, y_4) = a_4(t) + b_4(t) y_4 + c_4(t) y_4^2 \tag{50}$$

The boundary conditions for the wick of the bottom condenser section are

$$y_3 = 0, \quad q_{wv,\,c} = -k_w \frac{\partial \theta_{w,\,c}(t, y_3)}{\partial y_3} \tag{51}$$

$$y_3 = h_w, \quad \theta_{w,\,c}(t, y_3) = \theta_{ww,\,c}(t) \tag{52}$$

$$y_3 = h_w, \quad q_{ww,\,c}(t) = -k_w \frac{\partial \theta_{w,\,c}(t, y_3)}{\partial y_3} \tag{53}$$

and the boundary conditions for the heat pipe wall in the bottom condenser section are

$$y_4 = 0, \quad \theta_{wa,\,c}(t, y_4) = \theta_{ww,\,c}(t) \tag{54}$$

$$y_4 = \delta_4(t), \quad \theta_{wa,\,c}(t, y_4) = 0 \tag{55}$$

$$y_4 = \delta_4(t), \quad \frac{\partial \theta_{wa,\,c}(t, y_4)}{\partial y_4} = 0 \tag{56}$$

Applying boundary conditions, Eqs. (51)–(53), to Eq. (49) yields the temperature distribution in the wick of the bottom condenser section:

$$\theta_{w,\,c}(t, y_3) = \theta_{ww,\,c}(t) + \frac{\lfloor q_{wv,\,c}(t) + q_{ww,\,c}(t)\rfloor h_w}{2k_w} - \frac{q_{wv,\,c}(t)}{k_w} y_3 + \frac{\lfloor q_{wv,\,c}(t) - q_{ww,\,c}(t)\rfloor}{2k_w h_w} y_3^2 \tag{57}$$

Applying boundary conditions, Eqs. (54)–(56), to Eq. (50) yields the temperature distribution in the heat pipe wall in the evaporator section:

$$\theta_{wa,\,c}(t, y_4) = \theta_{ww,\,c}(t)\left(1 - \frac{y_4}{\delta_4(t)}\right)^2 \tag{58}$$

In determining the temperature distributions of the entire heat pipe, i.e., Eqs. (26), (42), (57) and (58), there are 7 unknowns, θ_{ww}, $e(t)$, q_{ww}, $e(t)$, $\theta_v(t)$, q_{wv},

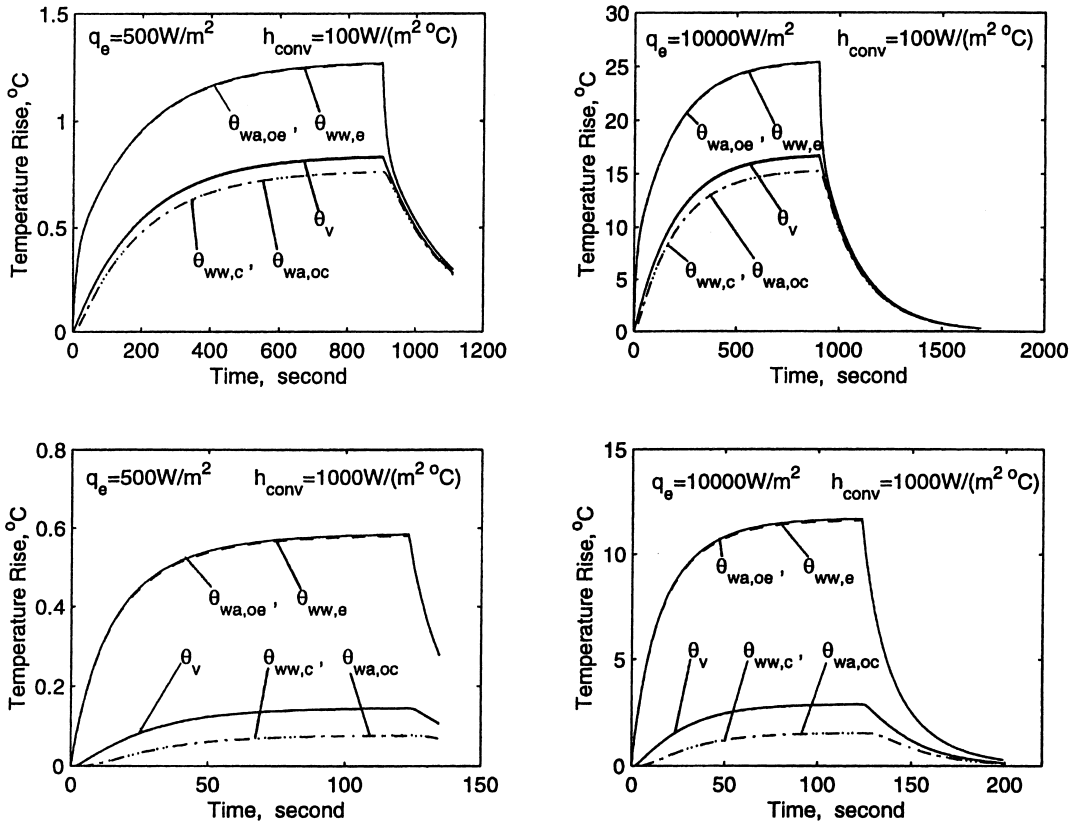

Fig. 3. Temporal temperature response within different pertinent sections of the flat plat heat pipe during startup and shutdown processes.

$c(t)$, θ_{ww}, $c(t)$, q_{ww}, $c(t)$, and $\delta_4(t)$. These seven unknowns can be determined by overall energy balances for the walls and the wicks of both evaporator and condenser sections and by the continuity of heat flux and temperature at the wick/wall interface. In the wick–vapor interface in the condenser section,

$$y_3 = 0, \quad \theta_{w,c}(t, y_3) = \theta_v(t) \tag{59}$$

Substituting Eq. (57) into (59), we have

$$\theta_v(t) = \theta_{ww,c}(t) + \frac{\lfloor q_{wv,c}(t) + q_{ww,c}(t) \rfloor h_w}{2k_w} \tag{60}$$

In the heat pipe wall–wick interface in the condenser section, the continuity of heat flux requires

$$y_4 = 0, \quad q_{ww,c}(t) = -k_{wa}\frac{\partial \theta_{wa,c}(t, y_4)}{\partial y_4} \tag{61}$$

Substituting Eq. (58) into Eq. (61) and rearranging, we have

$$q_{ww,c}(t) = \frac{2k_{wa}\theta_{ww,c}(t)}{\delta_4(t)} \tag{62}$$

The energy balance equation for the wick in the condenser section is

$$\int_0^{h_w} \frac{\partial \theta_{w,c}(t, y_3)}{\partial t}\, dy_3 = \int_0^{h_w} \alpha_w \frac{\partial^2 \theta_{w,c}(t, y_3)}{\partial y_3^2}\, dy_3 \tag{63}$$

Substituting Eq. (57) into (63) yields

$$\frac{d\theta_{ww,c}(t)}{dt} + \frac{h_w}{6k_w}\left[\frac{dq_{wv,c}(t)}{dt} + \frac{2dq_{ww,c}(t)}{dt}\right] = \frac{\alpha_w\left[q_{wv,c}(t) - q_{ww,c}(t)\right]}{k_w h_w} \tag{64}$$

The energy balance equation for the heat pipe wall of the condenser section is

$$\int_0^{\delta_4(t)} \frac{\partial \theta_{wa,c}(t, y_4)}{\partial t}\, dy_4 = \int_0^{\delta_4(t)} \alpha_{wa} \frac{\partial^2 \theta_{wa,c}(t, y_4)}{\partial y_4^2}\, dy_4 \tag{65}$$

Substituting Eq. (58) into Eq. (65) yields

$$\frac{d}{dt}\left[\delta_4(t)\theta_{ww,c}(t)\right] = \frac{6\alpha_{wa}\theta_{ww,c}(t)}{\delta_4(t)} \tag{66}$$

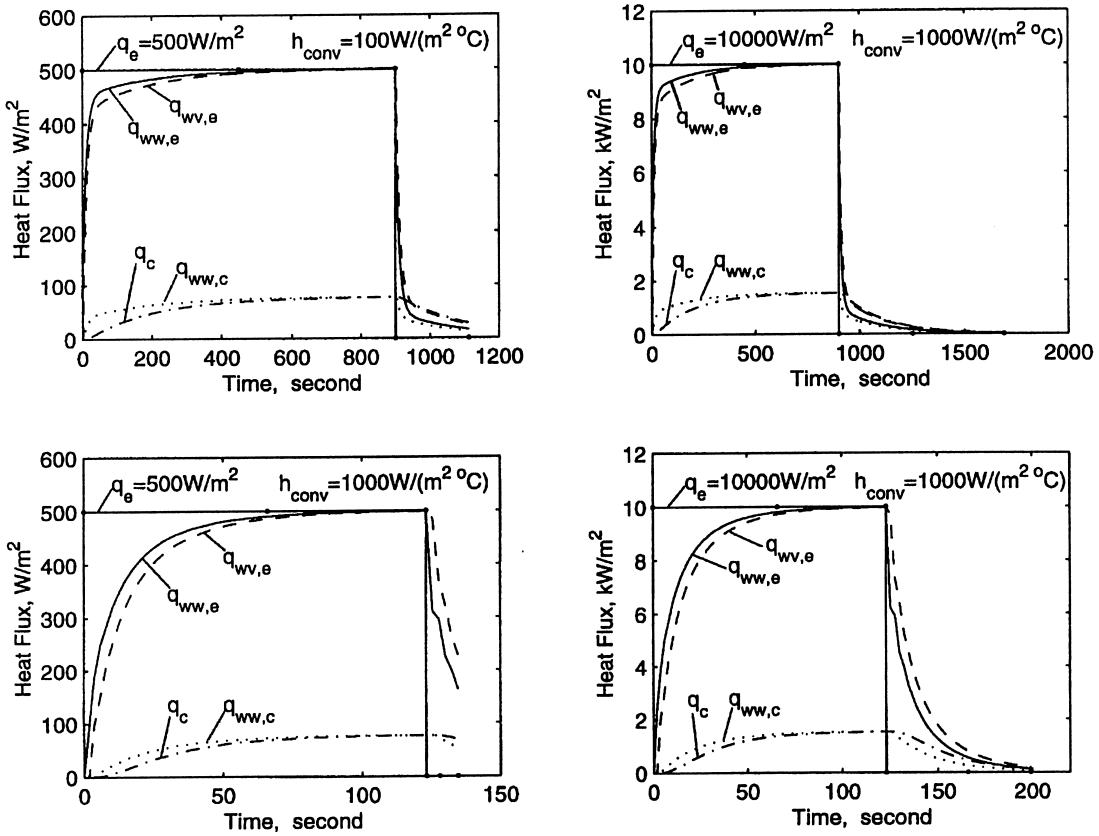

Fig. 4. Temporal power distribution throughout the flat plate heat pipe during startup and shutdown processes.

These seven unknowns can be determined by solving the system of Eqs. (33), (45), (46), (60), (62), (64) and (66). The temperature distribution for the whole heat pipe during this time period can be determined by Eqs. (26), (42), (57) and (58). It should be noted that the temperature distribution for the condenser was obtained for the lower condenser section, however, the obtained temperature distribution applies also to the upper condenser sections through a proper change of coordinate system.

3.4. Final passage of the thermal front through the heat pipe

During this step, the temperature distributions for the heat pipe wall and the wick in the evaporator section are prescribed by Eqs. (26) and (42), respectively, while the temperature distribution in the wick of the condenser section is described by Eq. (57). The temperature distribution in the heat pipe wall in the condenser section during this period is taken as

$$\theta_{\mathrm{wa,\,c}}(t, y_4) = a_4(t) + b_4(t)y_4 + c_4(t)y_4^2 \tag{67}$$

The corresponding boundary conditions are

$$y_4 = 0, \quad \theta_{\mathrm{wa,\,c}}(t, y_4) = \theta_{\mathrm{ww,\,c}}(t) \tag{68}$$

$$y_4 = 0, \quad q_{\mathrm{ww,\,c}}(t) = -k_{\mathrm{wa}}\frac{\partial \theta_{\mathrm{wa,\,c}}(t, y_4)}{\partial y_4} \tag{69}$$

$$y_4 = h_{\mathrm{wa}}, \quad -k_{\mathrm{wa}}\frac{\partial \theta_{\mathrm{wa,\,c}}(t, y_4)}{\partial y_4} = h_{\mathrm{conv}}\left[\theta_{\mathrm{wa,\,c}}(t, y_4) - \theta_\infty\right] \tag{70}$$

Applying boundary conditions, Eqs. (68)–(70), to Eq. (67) yields the temperature distribution in the wall of the lower condenser section (the same procedure is utilized for the upper condenser section)

$$\theta_{\mathrm{wa,\,c}}(t, y_4) = \theta_{\mathrm{ww,\,c}}(t) - \frac{q_{\mathrm{ww,\,c}}(t)}{k_{\mathrm{wa}}}y_4 + \frac{q_{\mathrm{ww,\,c}}(t)\left(1 + \dfrac{hh_{\mathrm{wa}}}{k_{\mathrm{wa}}}\right) - h_{\mathrm{conv}}\left[\theta_{\mathrm{ww,\,c}}(t) - \theta_\infty\right]}{(h_{\mathrm{conv}}h_{\mathrm{wa}} + 2k_{\mathrm{wa}})h_4}y_4^2 \tag{71}$$

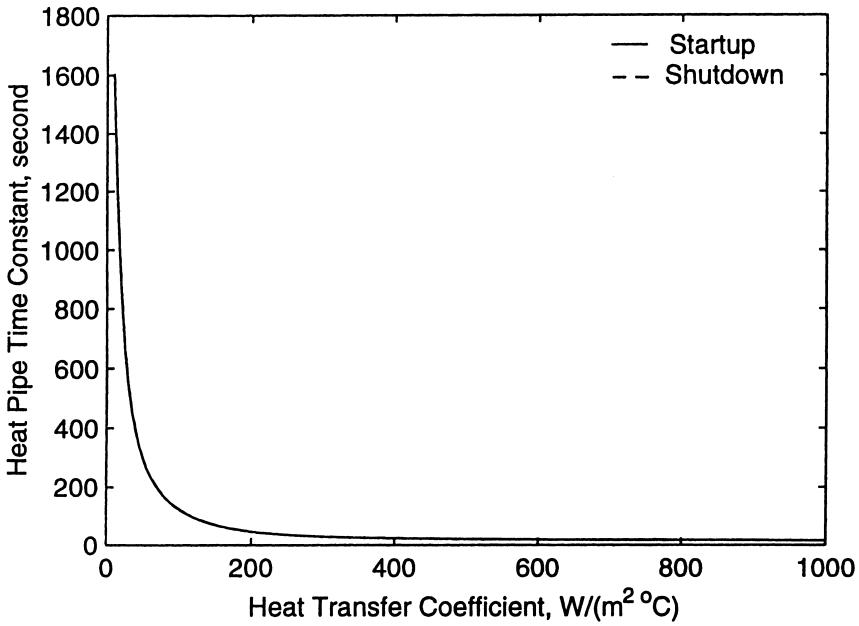

Fig. 5. Heat pipe time constant variations in response to changes in the heat transfer coefficient

Overall, energy balance for the wall of condenser section is

$$\int_0^{h_{wa}} \frac{\partial \theta_{wa,\,c}(t, y_4)}{\partial t}\,dy_4 = \int_0^{h_{wa}} \alpha_{wa} \frac{\partial^2 \theta_{wa,\,c}(t, y_4)}{\partial y_4^2}\,dy_4 \qquad (72)$$

Substituting Eq. (71) into Eq. (72) yields

$$\left[1 - \frac{h_{conv}h_{wa}}{3(h_{conv}h_{wa} + 2k_{wa})}\right]\frac{d\theta_{ww,\,c}(t)}{dt} + \left[\frac{h_{wa}}{3(h_{conv}h_{wa} + 2k_{wa})}\left(1 + \frac{h_{conv}h_{wa}}{k_{wa}}\right) - \frac{h_{wa}}{2k_{wa}}\right] \times \frac{dq_{ww,\,c}(t)}{dt} = \frac{\alpha_{wa}}{k_{wa}h_{wa}}\left\{1 - h_{conv}\left[\frac{h_{wa}}{h_{conv}h_{wa} + 2k_{wa}} \times \left(1 + \frac{h_{conv}h_{wa}}{k_{wa}}\right)\right]\right\} q_{ww,\,c}(t) - \frac{\alpha_{wa}h_{conv}}{k_{wa}h_{wa}} \times \left(1 - \frac{h_{conv}h_{wa}}{h_{conv}h_{wa} + 2k_{wa}}\right)\left[\theta_{ww,\,c}(t) - \theta_\infty\right] \qquad (73)$$

The temperature distributions after the final passage of the thermal front through the entire heat pipe are given by equations, (26), (42), (57) and (71). There are six unknowns in these equations (θ_{ww}, $e(t)$, q_{ww}, $e(t)$, $\theta_v(t)$, q_{wv}, $c(t)$, θ_{ww}, $c(t)$ and $q_{ww,\,c}(t)$). These unknowns can be determined by solving the system of Eqs. (33), (45), (46), (60), (64), and (73). The above described model uniquely establishes the temperature distribution within the entire heat pipe.

4. Model description during the shutdown operation

During the shutdown operation, the heat input is turned off resulting in a gradual decrease in the overall heat pipe temperature. A major difference between the shutdown and the startup operations is that during the former the temperature changes occur over the entire heat pipe at any given time and as such we no longer have to contend with the thermal penetration fronts as was the case in the startup operation.

The initial temperature distribution is known at any given time, based on the analytical results from the startup operation. As such this distribution is prescribed by a second-order polynomial. The boundary condition for the heat pipe wall in the evaporator section, Eq. (20), becomes

$$y_1 = 0, \quad \frac{\partial \theta_{wa,\,e}(t, y_1)}{\partial y_1} = 0 \qquad (74)$$

Incorporating Eq. (74) into (26) results in the temperature distribution in the heat pipe wall in the evaporator section during the shutdown operation

$$\theta_{wa,\,e}(t, y_1) = \theta_{ww,\,e}(t) + \frac{q_{ww,\,e}(t)h_{wa}}{2k_{wa}} - \frac{q_{ww,\,e}(t)}{2k_{wa}h_{wa}}y_1^2 \qquad (75)$$

Correspondingly, the energy balance equation (33) during the shutdown process changes to

$$\frac{d\theta_{ww,\,e}(t)}{dt} + \frac{h_{wa}}{3k_{wa}}\frac{dq_{ww,\,e}(t)}{dt} = \frac{\alpha_{wa}q_{ww,\,e}(t)}{k_{wa}h_{wa}} \qquad (76)$$

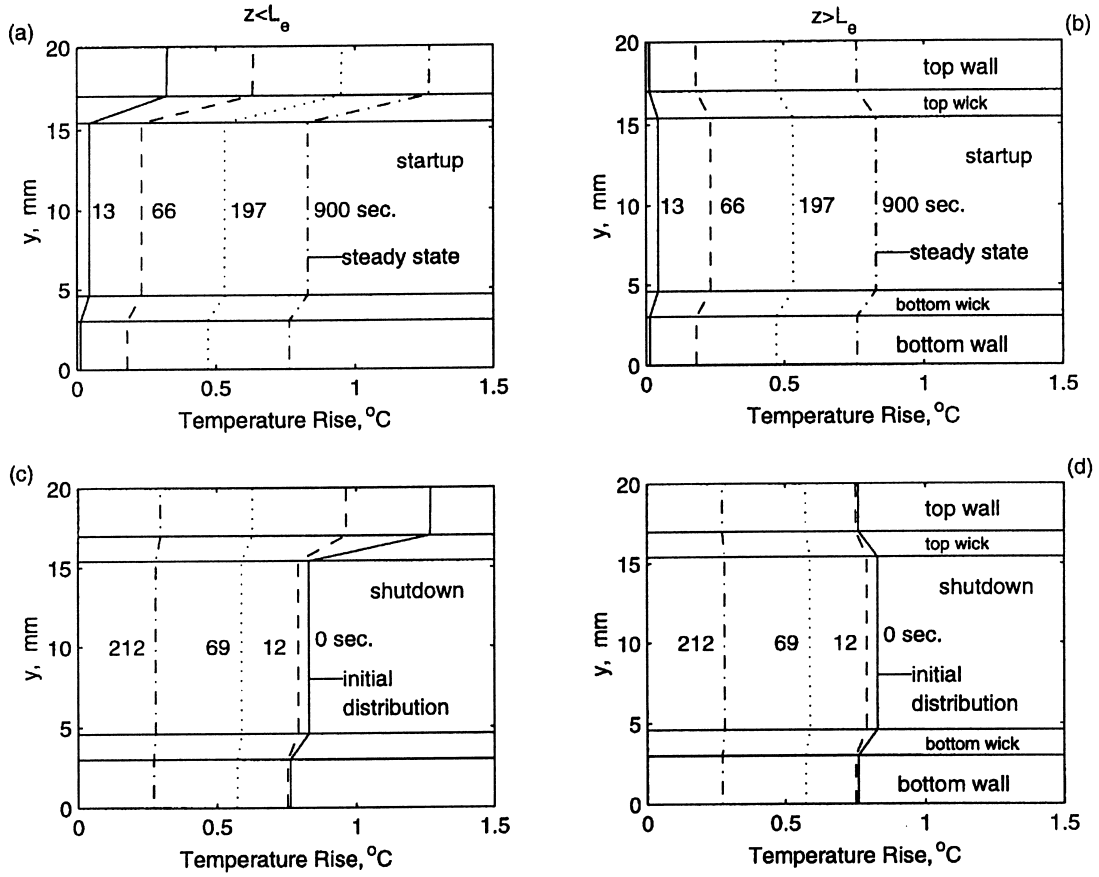

Fig. 6. Temperature distribution during the startup [(a) and (b)] and shutdown [(c) and (d)] operations for $h_{conv} = 100$ W/(m^2 °C) and $q_e = 500$ W/m^2.

The equation describing the temperature distribution for the wick in the evaporator section, Eq. (42), and the equations for the wick and the wall in the condenser section for the startup operation, Eqs. (57) and (71), are still available for the shutdown operation. The unknowns in these equations can be determined uniquely during the shutdown operation by utilizing Eqs. (45), (46), (60), (64), (73), and (76).

5. Physical characteristics of the system during the startup and shutdown processes

The temperature distribution and heat transfer for the startup and shutdown operations were simulated using the derived models described in the previous sections. In this work, steady state conditions are assumed to have been reached if the relative deviation between the input and output power is less than 0.2%, i.e,

$$1 - \lfloor h_{conv} A_c (\theta_{wa,\,oc} - \theta_\infty)/(q_e A_e) \rfloor < 0.002 \qquad (77)$$

Similarly, during the shutdown process, it is assumed that the heat pipe reaches its original temperature if the following criterion is met

$$\theta_{wa,\,oe} < 0.3°C \qquad (78)$$

The results show that raising the above cited convergence criteria does not have any significant effect on the obtained results. However, raising the criteria does increase the calculation time considerably.

At the start of the process, the original temperature of the heat pipe is uniform over the entire heat pipe and equals the temperature of the cooling fluid at the beginning of the startup operation. Similarly, in a shutdown operation, the temperature distribution within the heat pipe at the beginning of the shutdown process is known based on the results at the end of the startup operation. To simulate the entire transient performance involving the startup and shutdown operations, the temperature distribution of the heat pipe at the end of

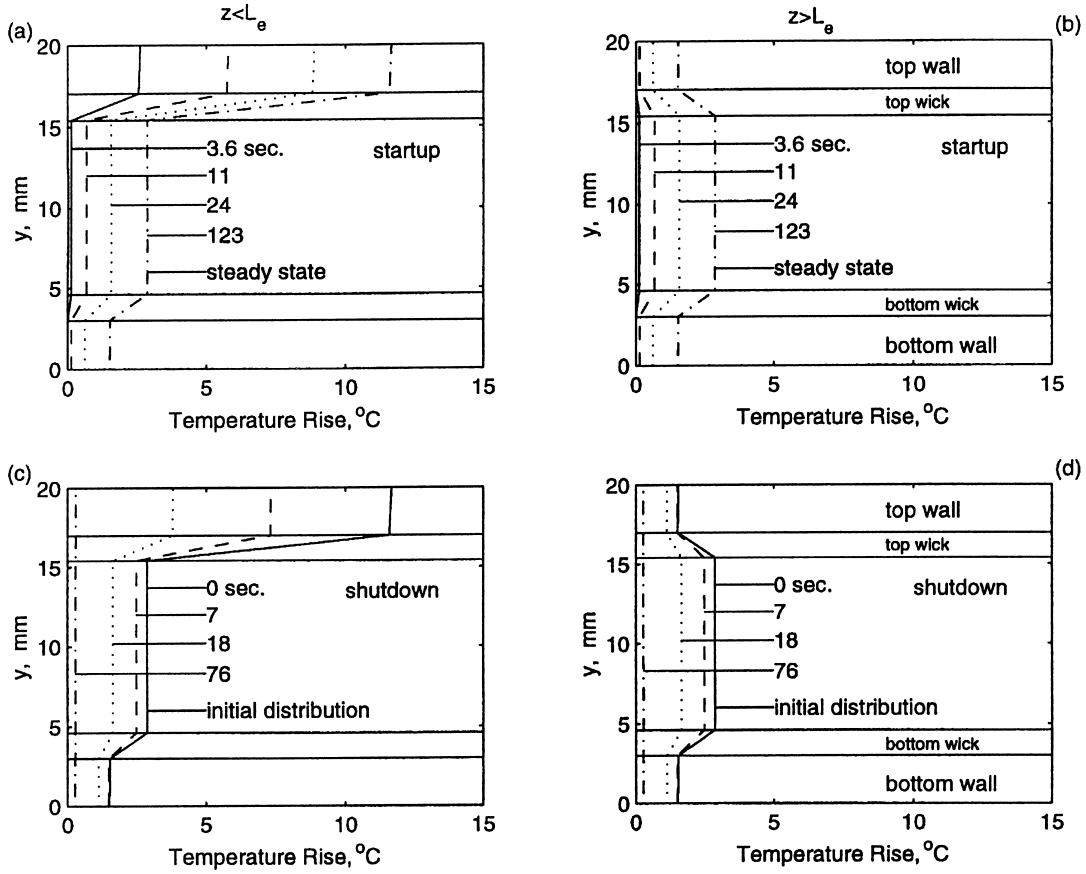

Fig. 7. Temperature distribution during the startup [(a) and (b)] and shutdown [(c) and (d)] operations for $h_{conv} = 1000$ W/(m^2 °C) and $q_e = 10{,}000$ W/m^2.

the startup operation is used as the initial temperature distribution for the shutdown process.

The heat pipe wall was taken as copper, while the wick was taken as sintered copper powder. The working fluid was taken as water. In this work, we are mainly interested in the effect of the heat input and the heat transfer coefficient on the performance of the heat pipe during the startup and shutdown processes. As such, the same geometrical configuration was used in all the cases studied in this work. In this work, the geometrical parameters of the heat pipe were taken as:

$h_{wa} = 3.0$ mm, $h_w = 1.6$ mm, $L = 95$ mm, $L_e = 25$ mm,

$W = 140$ mm, $H = 20$ mm, $\varepsilon = 50\%$

The heat transfer area in the condenser section is 7.5 times that of the evaporator section. The effective parameter of the wick are determined by [9]

$$k_w = k_{eff} = k_l\left[\frac{k_l + k_s - (1-\varepsilon)(k_l - k_s)}{k_l + k_s + (1-\varepsilon)(k_l - k_s)}\right] \tag{79}$$

$$\rho_{eff} = \varepsilon\rho_l + (1-\varepsilon)\rho_s \tag{80}$$

$$c_{eff} = \varepsilon c_l + (1-\varepsilon)c_s \tag{81}$$

$$\alpha_w = \alpha_{eff} = \frac{k_{eff}}{\rho_{eff} c_{eff}} \tag{82}$$

For a specified case, the input heat flux, heat transfer coefficient, and desired time interval are specified. The temperature distributions are then obtained based on the analytical model described in the earlier sections over different time periods. Once the steady state conditions, based on Eq. (77), are achieved at the end of the startup operation, this temperature distribution is used as an initial condition for the shutdown process. The shutdown process is carried on until the heat pipe

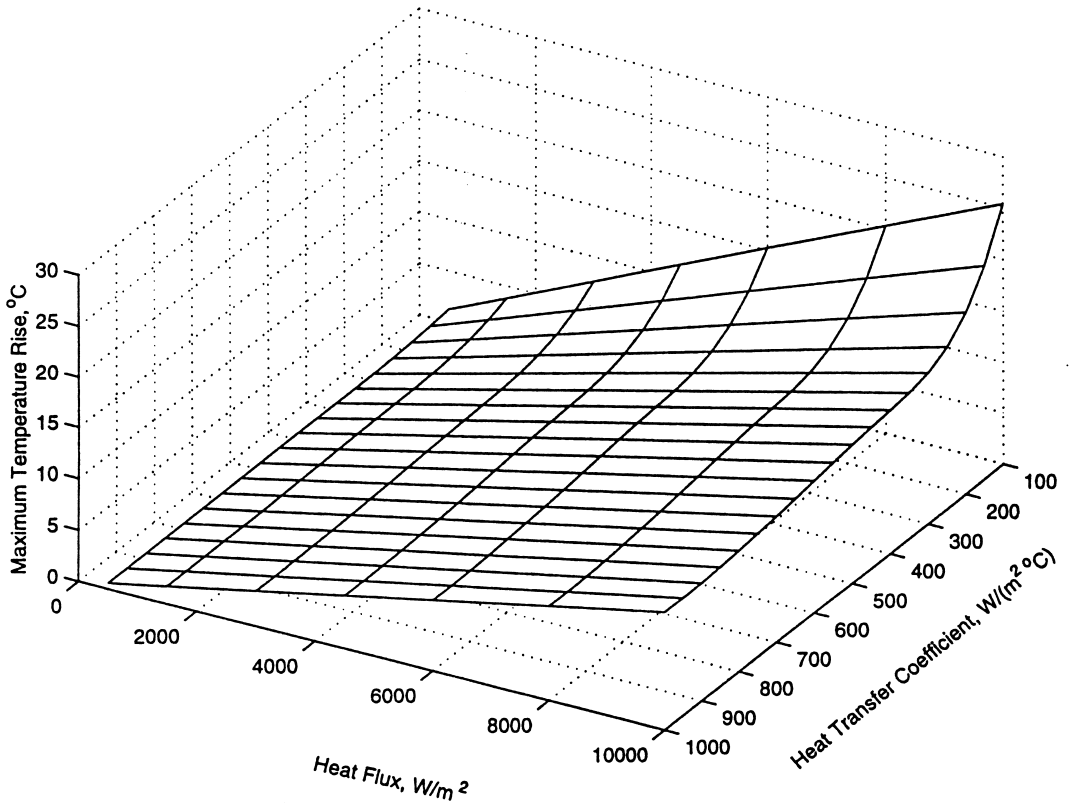

Fig. 8. Maximum temperature rise on the outside surface of the evaporator section.

reaches its original temperature as specified by Eq. (78).

In this work, simulations were performed accounting for heat transfer coefficient variations in the range of 10–1000 W/(m^2 °C) and input heat flux variations in the range of 500–10,000 W/m^2. It should be noted that presented analytical results are valid beyond the range of parameters utilized in the next section.

6. Results and discussion

The temporal temperature distributions at various locations within the flat plate heat pipe are displayed in Fig. 3 for four different sets of input power and outside heat transfer coefficients. The results indicate that the temperature difference within the heat pipe wall in either the evaporator or the condenser section is quite small. In fact, as can be seen in Fig. 3, it is difficult to observe the differences. The results also indicate that for a fixed thickness of a heat pipe wall or a wick, the time for the temperature front to penetrate through the heat pipe mainly depends on the thermal diffusivities of the wall and the wick and the heat transfer coefficient, and is slightly affected by the heat input level. However, the heat input pattern has a significant effect on the penetration time. For example, for a given wall or wick thickness, a linear heat input would increase the penetration time by three times compared with a constant heat flux input. A nonlinear heat input would increase the penetration time even further.

As can be seen in Fig. 3, the sharp increase in temperatures occurs in the initial heating period. Over the presented range, the input heat flux has no significant effect on the time it takes to reach steady state. For a specified flat plate heat pipe, the time to reach steady state depends mainly on the heat transfer coefficient. The larger the heat transfer coefficient, the smaller the time to reach steady state. For the cases presented in this work, the time to reach steady state varies from 947 s for $h_{conv} = 100$ W/(m^2 °C) to 133 s for $h_{conv} = 1000$ W/(m^2 °C). For a shutdown operation, all the temperatures throughout the heat pipe eventually approach a uniform initial temperature as shown in Fig. 3.

Fig. 4 shows the transient heat flux distribution

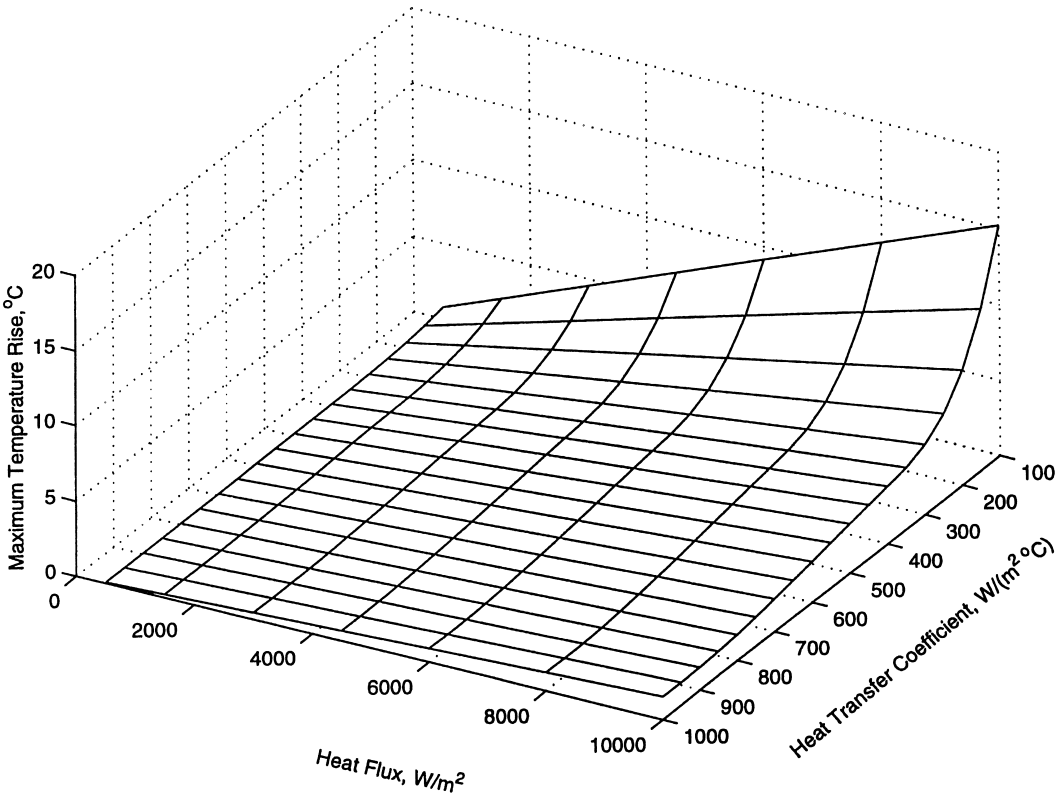

Fig. 9. Maximum temperature rise on the outside surface of the condenser section.

within different depths of the heat pipe for different heat input and heat transfer coefficients. As can be seen in Fig. 4, the heat fluxes at different locations in the evaporator section are quite close to each other except in the very beginning of the startup operation. Similar conclusions can be obtained for the condenser section. Heat flux approaches steady state faster than the transient temperature distribution during the startup operation. The same is true for the shutdown operation. As can be seen in Fig. 4, the heat pipe walls absorb more sensible heat than the wicks in both the evaporator section and the condenser section. When the input power is turned off, the heat flux at the wick–vapor interface exceeds that at the wall–wick interface in the evaporator section. For the condenser section, similar conclusions can be drawn, i.e., the heat flux at the wall–wick interface exceeds that in the wick–vapor interface and the heat flux on the outside wall surface exceeds that in the wall–wick interface. However, the evaporator section still maintains higher temperatures and the condenser section maintains lower temperatures in this operation. Experimental results related to thermal performance of flat-shaped heat pipes subject to passive air cooling is given in Wang and Vafai [10]. Detailed experimental transient characteristics of flat plate heat pipes during startup and shutdown operations and comparisons with the results presented in this work are given in Ref. [11]

In this work the idea of a heat pipe time constant is utilized for the startup operation. It is defined as the time when the outside surface temperature of the evaporator section reaches 63.2% of its maximum value. Similarly, a time constant for a shutdown operation is defined as the time when the outside surface temperature in the evaporator section drops 63.2% from its steady state value. These time constants can be used to determine how fast a heat pipe responds to an applied input power. For a specified heat pipe, the time constant depends mainly on the heat transfer coefficient. However, when the capacitance of the heat pipe is substantially increased, the heat input would affect the time constant very significantly. The dependence of the time constant on the heat transfer coefficient is displayed in Fig. 5. As can be seen in Fig. 5, when the heat transfer coefficient is relatively small, increasing the heat transfer coefficient can greatly reduce the time constant. However, for relatively large heat transfer coefficients, increasing the heat transfer coefficient has

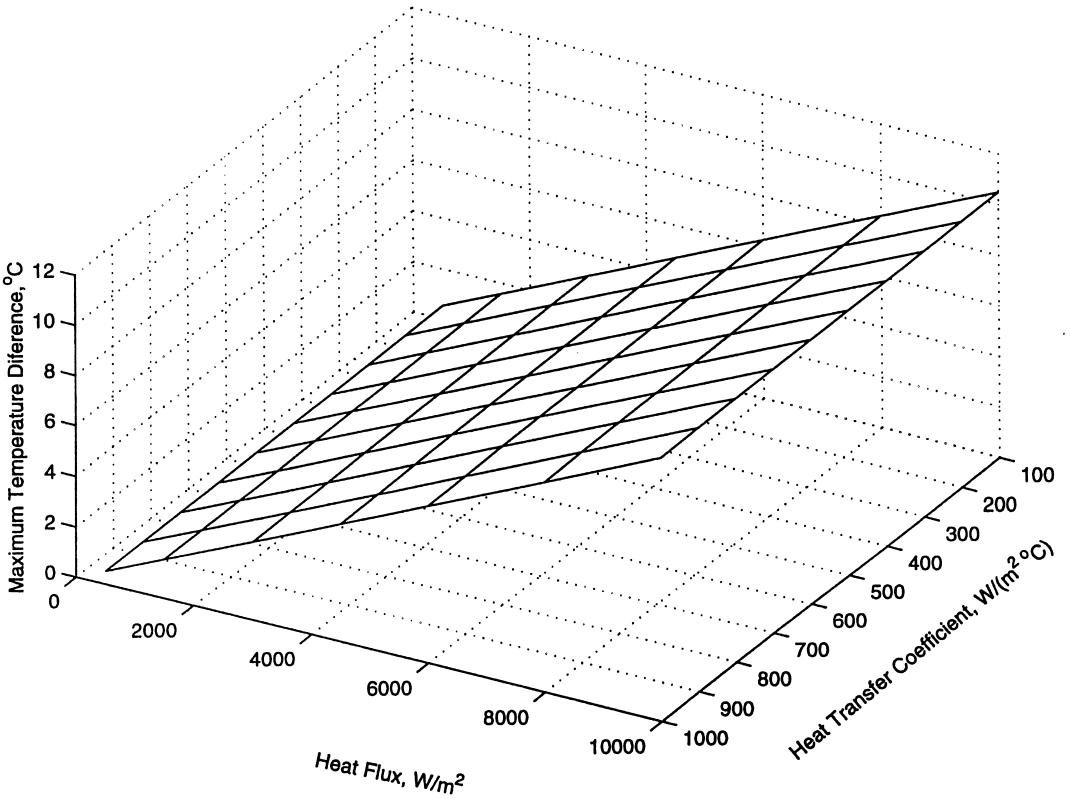

Fig. 10. Maximum temperature difference within the heat pipe.

an insignificant effect on the time constant. The results show that the time constant for the shutdown operation is very close to that for the startup operation. For example, when $h = 100$, the difference between the two time constants is only 1.6 s, or a relative deviation of 1.3%, and thus can be ignored.

Figs. 6 and 7 show the temperature distributions at different times for both startup and shutdown operations. As can be seen in Figs. 6 and 7, the maximum temperature drop takes place within the wick in the evaporator section. There is also a significant temperature drop within the wick in the condenser section. These two wicks contribute about 86 and 13% of the total temperature drop across the heat pipe within the evaporator section ($Z < L_e$). Also, as can be seen in Figs. 6 and 7, the temperature distribution is relatively more uniform in the shutdown operation (Figs. 6(c), (d) and 7(c), (d)) as compared to that during the startup operation (Figs. 6(a), (b) and 7(a), (b)). The line in Figs. 6 and 7 marked as steady state represents the temperature distribution at steady state for the startup operation, which is then used as the initial temperature distribution during the shutdown operation, as shown in Figs. 6(c), (d) and 7(c), (d). Once again, the porous wick in the evaporator section creates the largest thermal resistance across the heat pipe during the shutdown operation.

Figs. 8 and 9 show the maximum temperature rise on the outside wall surfaces for the evaporator and condenser sections. The maximum temperature rise indicates the highest temperature increase from the initial condition on the outside surface of the heat pipe. The maximum temperature rise increases linearly with the heat input, and decreases with an increase in the heat transfer coefficient. For relatively large heat transfer coefficients, further increase in the heat transfer coefficient decreases the maximum temperature rise only slightly; while for a relatively smaller heat transfer coefficient, increasing the heat transfer coefficient will reduce the maximum temperature rise significantly.

Fig. 10 shows the maximum temperature difference within the heat pipe. The maximum temperature difference refers to the maximum difference between the temperatures on the outside surface of the flat plate heat pipe. As can be seen in Fig. 10, the maximum temperature difference has a linear relationship with the heat input and has an insignificant dependence on

the heat transfer coefficient. However, it should be noted that although the heat transfer coefficient does not affect the maximum temperature difference within the heat pipe, it does affect the maximum outside surface wall temperatures on both the evaporator section and condenser section, as shown in Figs. 8 and 9.

7. Conclusions

Analytical models for predicting the transient performance of a flat plate heat pipe for both the startup and shutdown operations were developed in this work. This model can be utilized for both startup and shutdown operations. The presented model can simulate the thermal performance of a flat plate heat pipe in a cyclic startup and shutdown operation as well as other practical operation scenarios. The transient temperature distributions within the heat pipe walls and wicks were presented.

The results indicate that the thermal diffusivity and the thickness of the wall and the wick dominate the penetration time. Increasing the effective thermal diffusivity would decrease the penetration time. The results show that the heat transfer coefficient has a substantial effect on the heat pipe time constant. The results also show that the time constant for the startup operation is very close to that for the shutdown operation. Furthermore, the time for a specified flat plate heat pipe to reach steady state depends mainly on the heat transfer coefficient. Finally, it is found that the temperature difference within heat pipe walls is small and that the wick in the evaporator section creates the largest thermal resistance while the wick in the condenser section also has a significant contribution to the total thermal resistance.

Acknowledgements

The grant (DE-F602-93ER61612) by the Department of Energy is acknowledged and greatly appreciated.

References

[1] P.D. Dunn, D.A. Reay, Heat Pipes, 3rd ed., Pergamon Press, New York, 1982.
[2] M. Thomson, C. Ruel, M. Donato, Characterization of a flat plate heat pipe for electronic cooling in a space environment, in: National Heat Transfer Conference, Heat Transfer in Electronics, HTD-Vol. 111, 1989, 59–65.
[3] P.M. Sockol, R. Forman, Re-examination of heat pipe startup, in: Proceedings of the 9th IEEE Thermionic Conversion, 1970, pp. 571–573.
[4] J.M. Ochterbeck, Modeling of room-temperature heat pipe startup from frozen state, AIAA Journal of Thermophysics and Heat Transfer 11 (1997) 165–172.
[5] K. Vafai, W. Wang, Analysis of flow and heat transfer characteristics of an asymmetrical flat plate heat pipe, International Journal of Heat Mass Transfer 35 (1992) 2087–2099.
[6] K. Vafai, N. Zhu, W. Wang, Analysis of asymmetrical disk-shaped and flat plate heat pipes, ASME Journal of Heat Transfer 117 (1995) 209–218.
[7] N. Zhu, K. Vafai, Vapor and liquid flow in an asymmetrical flat plate heat pipe: a three-dimensional analytical and numerical investigation, International Journal of Heat Mass Transfer 41 (1998) 159–174.
[8] N. Zhu, K. Vafai, Analytical modeling of the startup characteristics of asymmetrical flat plate and disk-shaped heat pipes, International Journal of Heat and Mass Transfer 41 (1998) 2619–2637.
[9] S.W. Chi, Heat Pipe Theory and Practice, Hemisphere, Washington, 1976.
[10] Y. Wang, K. Vafai, An experimental investigation of the thermal performance of an asymmetrical flat plate heat pipe, International Journal of Heat and Mass Transfer 43 (2000) 2657–2667.
[11] Y. Wang, K. Vafai, An experimental investigation of the transient characteristics of a flat plate heat pipe during startup and shutdown operations, accepted for ASME Journal of Heat Transfer.